A&A 488, 675–684 (2008)
DOI: 10.1051/0004-6361:200809932

Astronomy & Astrophysics

Infrared photometry and evolution of mass-losing AGB stars

II. Luminosity and colors of MS and S stars⋆,⋆⋆

R. Guandalini and M. Busso

Department of Physics, University of Perugia, and INFN, Sezione di Perugia, via A. Pascoli 1, 06123 Perugia, Italy
e-mail: [guandalini;busso]@fisica.unipg.it

Received 8 April 2008 / Accepted 24 June 2008

ABSTRACT

Context. Asymptotic giant branch (AGB) phases mark the end of the evolution for low- and intermediate-mass stars. Our understanding of the mechanisms through which they eject the envelope and our assessment of their contribution to the mass return to the interstellar medium and to the chemical evolution of Galaxies are hampered by poor knowledge of their luminosities and mass loss rates, both for C-rich and for O-rich sources.
Aims. We plan to establish criteria permitting a more quantitative determination of luminosities (and subsequently of mass loss rates) for the various types of AGB stars on the basis of infrared fluxes. In this paper, in particular, we concentrate on O-rich and *s*-element-rich MS, S stars and include a small sample of SC stars.
Methods. We reanalyze the absolute bolometric magnitudes and colors of MS, S, SC stars on the basis of a sample of intrinsic (single) and extrinsic (binary) long period variables. We derive bolometric corrections as a function of near- and mid-infrared colors, adopting as references a group of stars for which the spectral energy distribution could be reconstructed in detail over a large wavelength range. We determine the absolute HR diagrams, and compare luminosities and colors of S-type giants with those, previously derived, of C-rich AGB stars. Luminosity estimates are also verified on the basis of existing period-luminosity relations valid for O-rich Miras.
Results. S star bolometric luminosities are almost indistinguishable from those of C-rich AGB stars. On the contrary, their circumstellar envelopes are thinner and less opaque. Despite this last property the IR wavelengths remain dominant, with the bluest stars having their maximum emission in the H or K(short) bands. Near-to-mid infrared color differences are in any case smaller than for C stars. Based on period-luminosity relations for O-rich Miras and on Magnitude-color relations for the same variables we show how approximate distances (hence intrinsic parameters) for sources of so far unknown parallax can be inferred. We argue that most of the sources have a rather small mass (<2 $M_{\odot}$); dredge-up might then be not effective enough to let the C/O ratio exceed unity.

Key words. stars: fundamental parameters – stars: AGB and post-AGB – stars: evolution – infrared: stars – stars: variables: general

1. Introduction

The asymptotic giant branch phases (hereafter AGB) represent the second ascent along the red giant branch, occurring after the exhaustion of core He burning for all stars between ∼0.8 and 8.0 $M_{\odot}$. In these evolutionary stages, stars are powered by two nuclear shells, burning H and He alternatively. In particular, in the final 1−2 Myr of the AGB, the He-burning shell remains mainly quiescent, if not for recurrent explosive ignitions during which a lot of C (from 20 to 25% by mass) is produced and spread over the whole He-rich layer, in short phases of convective mixing (the so-called *thermal pulses*). Convective penetration of the envelope follows, in repeated episodes collectively called "the third dredge-up", and carries the new carbon to the surface, together with other nucleosynthesis products, in particular *s*-elements generated by efficient neutron captures (Busso et al. 1999).

Due to the above phenomena, the atmospheres of AGB stars are characterized by an increasing enrichment of ^{12}C (up to C/O > 1 by number, in which case we speak of C stars) and of *s*-process nuclei, in particular revealing the recent nucleosynthesis through the short-lived ^{99}Tc (Merrill 1952). Sometimes Tc itself offers actually the only real evidence of ongoing *s*-processing in stars that do not show other remarkable chemical anomalies (Uttenthaler et al. 2007). When instead the third dredge-up process is efficient enough, changes in the photospheric abundances of other *s*-elements begin to occur, first of all for Zr, which has various isotopes on the main *s*-process path. In such cases the appearance of ZrO bands in the spectra (at wavelengths 464.1, 462.0, 530.4, 537.9, and 555.1 nm) tells us that the star, although still richer in O than in C, is mixing to the surface the products of shell-He burning. The cool giants presenting these signatures are called MS and S stars (the second group showing more prominent features). They also have a C/O abundance ratio by number higher than in the Sun, but lower than unity. There is still some confusion about the exact values of the C/O ratios in MS and S stars, which is mainly induced by the remaining uncertainty in the calibrating solar oxygen abundance. If one excludes for this calibration the recent, still debated suggestion (Allende Prieto et al. 2002) and adopts instead the previous more traditional reference (Anders & Grevesse 1989), then MS stars are found typically at C/O = 0.5 to 0.7, and S stars are found above this range and up to more than 0.95. Around the border between O-rich and C-rich giants, the so-called SC stars represent a rare, but important, transition group.

In some cases, red giants showing *s*-element enhancement are Tc-poor. This is a clear indication that a sufficiently long time interval has passed since the production of neutron capture nuclei, so that Tc has decayed. In general, this is the case when

⋆ Tables 1–10 are only available in electronic form at http://www.aanda.org

⋆⋆ Tables 11 and 12 are only available in electronic form at the CDS via anonymous ftp to cdsarc.u-strasbg.fr (130.79.128.5) or via http://cdsweb.u-strasbg.fr/cgi-bin/qcat?J/A+A/488/675

the nucleosynthesis phenomena occurred not in the same star we see today, but in a more massive companion, which is now evolved to the white dwarf stage, and whose mass loss enriched in the past the photosphere of the observed object (Busso et al. 2001). In these cases we speak more properly of an *extrinsic* AGB star (Smith & Lambert 1990).

AGB stars lose mass very effectively, and their winds replenish the interstellar medium (ISM) guaranteeing up to 70% of the mass return from stars (Sedlmayr 1994). Before being dispersed over the Galaxy, the material thus lost forms cool envelopes (Winters et al. 2003) where dust grains condense (Carciofi et al. 2004). These solid particles carry the elemental and isotopic composition generated by AGB nucleosynthesis; they have been found in ancient meteorites offering the possibility of high precision isotopic abundance measurements on matter coming from circumstellar environments (e.g. Zinner 2000).

The cool AGB photospheres radiate most of their flux at red-infrared wavelengths. The infrared component of the spectral energy distribution (SED) grows in importance (and in average wavelength) as far as the evolution proceeds, because of the increased extinction of the photospheric flux operated by dust, which then re-radiates at long wavelengths (see e.g. Habing 1996). This correlation between extinction and evolutionary stage is however confused by the stars switching from Semiregular to Mira-type surface variability, which fact modulates the mass loss efficiency and hence the extinction properties. Due to these complicacies, large surveys of infrared (IR) observations play a fundamental role in studying luminosities and mass loss rates of AGB stars and in disentangling the variability and evolution effects (see e.g. Wood & Cohen 2001; Le Bertre et al. 2001, 2003; Groenewegen et al. 2002; Cioni et al. 2003; Omont et al. 2003; Olofsson et al. 2003).

Longstanding efforts have been devoted to describe the mass loss mechanisms, either with phenomenological models or with sophisticated hydrodynamical approaches (Salpeter 1974; Knapp & Morris 1985; Winters et al. 2003; Wachter et al. 2002; Sandin & Höfner 2003a,b). Despite this, our quantitative knowledge of AGB winds is still poor and forces us to adopt parametric treatments, where observations play a crucial role in fixing the (otherwise free) parameters (Wood 2003; Olivier & Wood 2003; Wood et al. 2004; Andersen et al. 2003).

Similar problems affect the estimates of the stellar luminosity. Observations are hampered by the difficulties of measuring the distances for single, often obscured objects like AGB stars. On the other hand, the luminosities derived from full stellar evolutionary models are affected by the uncertainties in the choice of the mixing parameters (in particular of the extension of convective overshoot) and of surface atomic and molecular opacities (Marigo et al. 2003). Models adopting large overshoot parameters (see e.g. Izzard et al. 2007) derive large values for the mass dredged-up after each thermal pulse, thus obtaining the surface enrichment in C and *s*-elements earlier and at a lower luminosity than models based on the Schwarzschild's criterion can do.

In a previous paper of this series, hereafter referred to as "Paper I" (Guandalini et al. 2006), we analyzed a sample of C stars reconstructing their SEDs up to far infrared, on the basis of space-borne infrared observations from the ISO and MSX missions. We found evidence for a relatively large average C-star luminosity, thus suggesting that the so-called "C-star luminosity problem" (Cohen et al. 1981) might not be real, being simply an effect of poor estimates of the luminosity, due to insufficient knowledge of the mid-infrared emission. We also reviewed the available mass loss rates and showed their correlation with infrared colors.

We want now to extend that analysis, considering those thermally-pulsing AGB stars where the enhancement of C (and *s*-elements) is more moderate than in C stars: it is the case of MS and S giants (Busso et al. 1992, 1995). In Sect. 2 we present the sample stars, and we discuss the choices made in selecting and organizing them in sub-samples, according to the quality of the available data. In Sect. 3 we present the IR colors and derive the bolometric corrections, based on a set of sources whose magnitude can be estimated safely through the integral of detailed SEDs. We also use these corrections for inferring the critical parameters (absolute magnitudes or distances) of sources for which either i) we have incomplete IR coverage but reliable distance estimates; or ii) period-luminosity relations yield the luminosity, and the distance needs to be inferred from the distance modulus. (For the sake of clarity, the adopted period-luminosity relations are discussed in Appendix A.) Once the absolute magnitudes are known, in Sect. 4 we can analyze HR diagrams and luminosity functions and on this base we also attempt a rough estimate of photometric parallaxes for Mira variables with no other available data on luminosities. Then, in Sect. 5 some preliminary conclusions are derived, while we postpone to a forthcoming dedicated work the analysis of stellar winds.

2. The sample of S stars

We started from the extended lists by Stephenson (Stephenson 1984, 1990), containing O-rich evolved red giants with known or suspected "S star-like" chemical peculiarities. As mentioned, these last anomalies can be due either to in-situ dredge-up of newly produced elements (intrinsic-S stars) or to mass-transfer episodes in a binary system (extrinsic-S stars). From those catalogues we selected a total of 613 sources for which measurements in the near-IR are available (from 2MASS, see Cutri et al. 2003). Another required property for selection was the existence of mid-infrared photometry (although with varied detail and spectral coverage). The chosen sources fall into various categories, depending on the extension and quality of the information we could collect on their IR colors, distance, variability type, period, luminosity. As a result, we can organize the stars selected in the following four sub-samples:

– **Sub-sample** *A*. This contains 21 sources for which ISO-SWS measurements exist up to long wavelengths (40–45 μm), so that a detailed SED can be obtained. The mid-IR SEDs can then be integrated together with near infrared photometric points, in order to infer a very reliable (apparent) bolometric magnitude, by means of the relations of fundamental photometry (Glass 1999; see also Paper I). In this way we have a means for computing bolometric corrections and look for their correlations with available parameters. Much like for C stars (Paper I), these bolometric corrections are correlated to near-to-mid infrared color indexes. About 50% of the stars in sub-sample *A* have also astrometric estimates of the distance from the revised Hipparcos catalogue (van Leeuwen 2007a,b); for some others we could infer a distance from the variability period. In all such cases, also the *absolute* magnitudes can be obtained: the stars with these characteristics are therefore the fundamental bricks on which we build the rest of our work. In particular, bolometric corrections offer us the tools for deriving absolute bolometric magnitudes for AGB stars outside this main sub-sample *A*, whenever observations of at least one near-to-mid color index exist.

– **Sub-sample** *B*. Here we put all sources (21) for which a reliable estimate of the distance is available (e.g. from Hipparcos, especially after the recent revision by van Leeuwen 2007a,b), but a detailed mid-infrared SED is not present. Although the stars of sub-sample *B* have only sparse mid-infrared photometry (from MSX, IRAS-LRS or ground-based measurements), thanks to the bolometric corrections discussed above absolute bolometric magnitudes can be computed for all of them.
– **Sub-sample** *C*. This class contains 41 Mira-type stars, for which near-to-mid IR colors could be derived from either MSX or IRAS measurements. Their Mira variability, of known period, allows for the application of period-luminosity relations, yielding the absolute luminosities (see in particular Whitelock et al. 2008). Some comments on the procedure used in this case to homogenize period-luminosity relations are presented in Appendix A. By also applying the bolometric corrections computed from sub-sample *A* to their photometric data, the apparent bolometric magnitudes can be derived, so that an estimate for the distance can be inferred from the distance modulus.
– **Sub-sample** *D*. Here we collect all the remaining sources (∼500). One or a few measurements at mid-infrared wavelengths exist also for this sub-sample; these data can be coupled to 2MASS photometry, giving near-to-mid infrared colors on which to apply the bolometric corrections. In this way, we can at least derive reliable bolometric (apparent) magnitudes. As the distance is in general not known from measurements (unlike for sub-sample *B*), and neither it can inferred from any known period (unlike for sub-sample *C*), a precise value for the absolute magnitude cannot be given at this stage and will have to wait for estimates of the distance. However, we shall see that, at least for known Mira variables, fiducial intervals for the distance can be derived from the HR diagram and the luminosity functions, in the form of a rough photometric parallax.

The first three samples, together with the input data we shall analyze for them, and the resulting estimates for their fundamental parameters are placed in the "online material" as Tables 1 to 9. The tables of the last sample are available electronically at the CDS.

In general, we perform the same kind of analysis already presented in Paper I for C-rich AGB stars, computing the bolometric corrections and bolometric apparent magnitudes, the absolute magnitudes when possible, and expressing the color data in the photometric system described in Paper I and in Busso et al. (2007), hereafter Paper II. In order to adopt this photometric system, we need to perform a re-binning of space-borne spectroscopic data, by convolving them with the response of the filters. We then discuss luminosities and luminosity functions for understanding the evolutionary relations between S stars and C stars along the thermally-pulsing AGB.

3. Infrared colors and bolometric corrections

We have made a preliminary control that the choice of near and mid IR wavelengths is sufficient for our scope. In fact, one might a priori believe that the inclusion of optical bands could increase the accuracy of bolometric corrections (despite the large uncertainties related to the photospheric variability). However, for all the stars of our samples for which we could find archived visual magnitudes, the optical-to-near-IR colors (e.g. $V - J$) are always in excess of 3 mag. Most $V - J$ colors lay in the range 4−7 and a few in the range 7−10 mag, implying flux ratios f_J/f_V larger than at least a factor of 10 and more often a factor of 100. There would be therefore no significant change in the results by introducing optical photometric data. S stars are certainly bluer than C stars (only a couple of sources are dominated by mid-IR, as is instead common for C-rich Miras, like CW Leo); but even when the infrared excess by dust is minimal and the photospheres are optically bright, all AGB stars, including S stars, remain mainly IR objects. The bluest of our sources have maximum emission in the *H* band.

As discussed in the previous section, we then start from the sources of sub-sample *A* in order to derive the bolometric corrections, then proceed to the other stars in our selection. The relevant parameters we collect or derive can be divided into three categories, so we have three tables per each sub-sample.

Table 1 presents the general characteristics of sub-sample *A*. This includes: i) the names of the sources (from IRAS, from the Stephenson's compilation (Stephenson 1984, 1990) and, when available, from the variable star nomenclature); ii) the coordinates (with the equinox fixed at year 2000.0) as given by the ICRS on the SIMBAD database; iii) the spectral types; and iv) the variability type, according to the General Catalogue of Variable Stars (GCVS, Samus et al. 2004). Some of the stars we analyze have uncertain spectral classifications for various reasons. As this point is not among the main issues we want to address, in all these cases we indicate the alternative choices found in the literature, simply separating them by a slash (/). In some cases, our analysis will yield suggestions on the correct classification.

The ISO-SWS SEDs of a few sources of group *A* are shown in Fig. 1, organized according to their spectral classification (MS or S) and variability type (Mira, Semiregular or Irregular). The figure shows one of the most evident properties of AGB stars, present also in C- rich sources: the Mira-type variability is often associated with a remarkable IR excess and a SED peaked at longer wavelengths than for Semiregular or Irregular variables. As compared to C stars, however, the IR excess of S stars is in general much smaller, as we already mentioned. This is probably related to intrinsic properties of dust with O-based or C-based composition. A similar difference exists for molecules (e.g. gaseous component) of the two species, as seen from the photospheres, as we shall argue later.

The above very detailed energy distributions are integrated to estimate the apparent bolometric magnitude, using the relation:

$$m_{\rm bol} = -2.5 \int_0^\infty f_\nu {\rm d}\nu + C \qquad (1)$$

as discussed by Glass (1999), who also gives $C = -18.98$ in the case where the total flux is expressed in W m^{-2}. This relation also provides the zero-magnitude flux. From Eq. (1) one obtains:

$$f_0 = \int_0^\infty f_\nu {\rm d}\nu = 1.94 \times 10^{-7}\ {\rm W\,m^{-2}} = 1.94 \times 10^{19}\ {\rm Jy\ Hz}. \qquad (2)$$

Following the procedure described in Papers I and II, we again operate a re-binning of the ISO spectra to derive estimates for the fluxes in a number of broader-band infrared filters (with 10% bandwidth), in the range between 8 and 14 μm (centered at 8.8, 9.8, 11.7 and 12.5 μm). (The fluxes in such filters are usually indicated as the equivalent wavelengths in normal brackets; the magnitudes use a similar notation but with squared brackets). These filters are of rather common use in ground-based infrared cameras; our choice is aimed at making the space-borne measurements more easily comparable with present and future

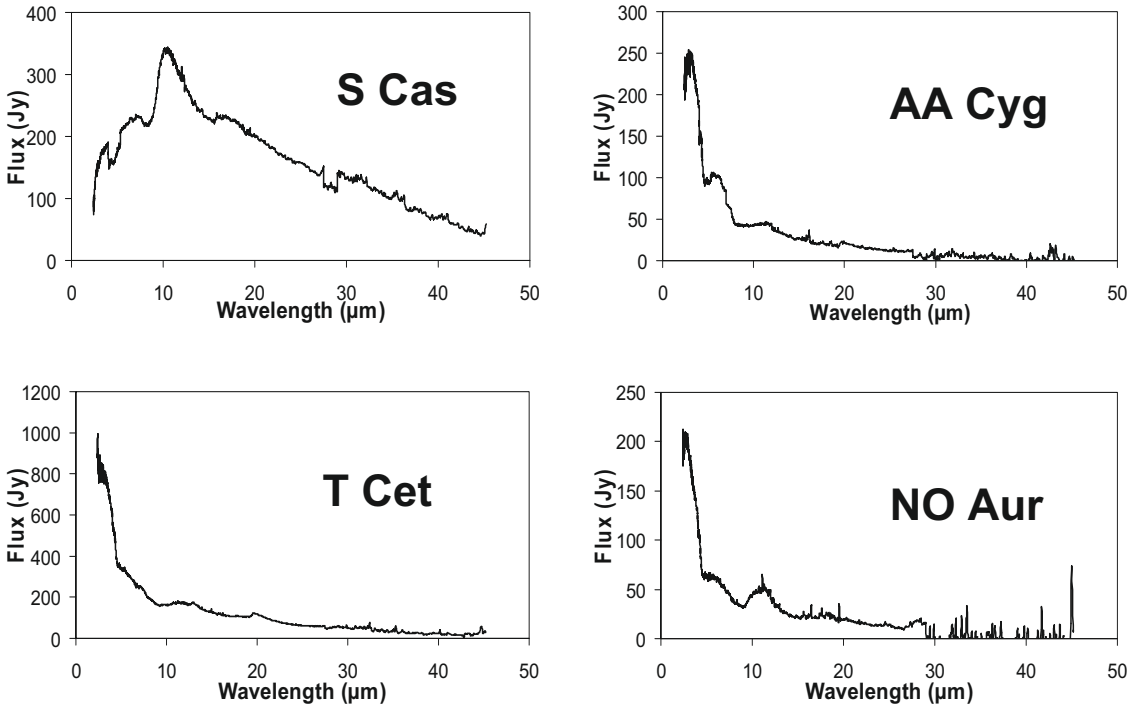

Fig. 1. Examples of ISO-SWS spectra of AGB stars. *Upper left*: a S-type Mira variable (S Cas). *Upper right*: a S-type Semiregular source (AA Cyg). *Lower left and right*: two MS stars.

photometric observations and to infer for these last suitable bolometric corrections. At long wavelengths ($\lambda > 14$ μm) the re-binning is made using the response curve of the MSX filters D (14.6 μm) and E (21.3 μm). Zero-magnitude fluxes (in Jy) for our chosen photometric system are: 52.23 (8.8 μm), 42.07 (9.8 μm), 29.55 (11.7 μm), 25.88 (12.5 μm), 20.25 (14.6 μm), 8.91 (21.3 μm). For near-IR, 2MASS calibrations for the J, H and K_s filters are given in Cohen et al. (2003). (Hereafter we shall adopt for the K "short" K_s filter the simple notation K.)

Figure 2 gives some examples of the SEDs computed in the photometric system thus defined, for the various types of AGB stars discussed in this note. The same data are listed in Tables 2, 5 and 8, together with near-infrared fluxed obtained from the 2MASS catalogue.

As a consistency check, we repeated the calculations of Eq. (1) using the apparent bolometric magnitudes previously derived from ISO spectra, and making the integral over the low-resolution SEDs of Fig. 2. By adopting the zero-magnitude fluxes by Bessell et al. (1998), we obtain for the integration constant an average value $C = -19.0$. The fact that this estimate be very close to the real C value given above certifies that the our re-binning is done properly, and does not alter in any significant way the integrals of Eq. (1), hence the magnitudes of our stars.

Once the apparent bolometric magnitudes are known, for those sources for which a reliable estimate of the distance exists we can derive M_{bol}. This estimate can be obtained also for those Mira variables of sub-sample A for which an astrometric measurement of the distance is not available, but the variability period is known. Indeed, the period-luminosity relations of Mira stars have become sufficiently reliable that we can use them to infer M_{bol} and then obtain the distance from the distance modulus (see Appendix A). The limit of this technique lays in the fact that, not having a proper description of the interstellar extinction, we are forced to exclude the extinction correction. The error introduced on infrared colors, however, is not large, and the related uncertainty remains within the (broad) observational errors of typical infrared photometry (see Paper I for a discussion).

Table 3 presents the absolute bolometric magnitudes derived for sub-sample A, with the indication of the method used, i.e. period-luminosity relations (labeled "this paper") or distances in the literature (labeled after the reference adopted, either "Hipparcos", see van Leeuwen 2007a; or in a single case "Groenewegen", taken from Groenewegen et al. 2002). The values adopted for either the period or the distance are also indicated.

We can then correlate the newly found bolometric magnitudes with color indexes in the infrared, in order to infer bolometric corrections to be applied to the other groups of stars in our sample. In Fig. 3 we present two of the most significant such correlations. They are shown as corrections to a mid-infrared magnitude ([8.8] or [12.5]) as functions of near-to-mid infrared color indexes ($K - [8.8]$ or $K - [12.5]$ respectively). Least-square fits, shown in the panels of the figure, correspond to:

$$\text{B.C.} = -0.0118 \cdot (K - [8.8])^2 + 1.1552 \cdot (K - [8.8]) + 2.3061 \quad (3)$$

and to

$$\text{B.C.} = -0.0195 \cdot (K - [12.5])^2 + 1.1949 \cdot (K - [12.5]) + 2.1918 \quad (4)$$

with correlation coefficients of $R = 0.990$ and $R = 0.993$, respectively.

As shown in the figures, both relations are quite tight and offer a reliable way to estimate absolute bolometric magnitudes for stars for which we have only partial photometric coverage. In the two plots of Fig. 3, there is only one point which is significantly discrepant and does not follow the average correlation. Quite significantly, this point corresponds to II Lup, a star that, although listed in the Stephenson's compilation of S stars, is instead a carbon-rich Mira variable and must therefore be excluded in discussing the photometric properties of O-rich AGB stars.

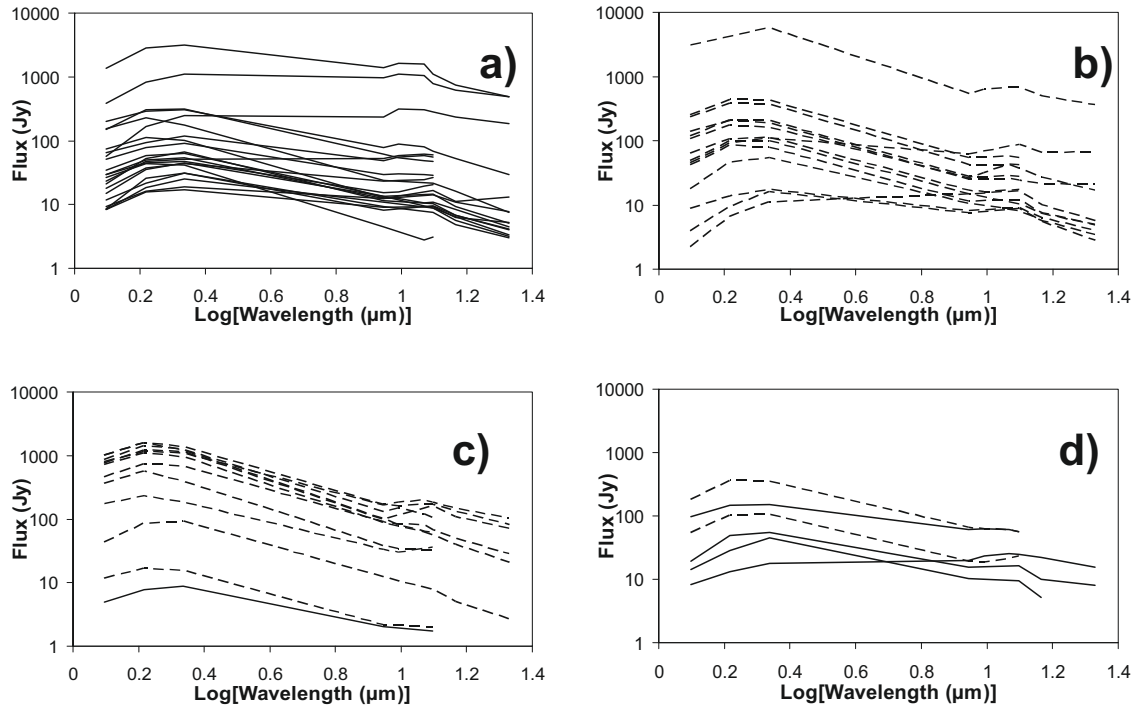

Fig. 2. Spectral energy distributions of sample stars after rebinning in the photometric system of Paper I. **a)** S Miras. **b)** S Semiregulars. **c)** MS sources. **d)** SC stars. Continuous lines refer to Miras, dashed ones to Semiregulars.

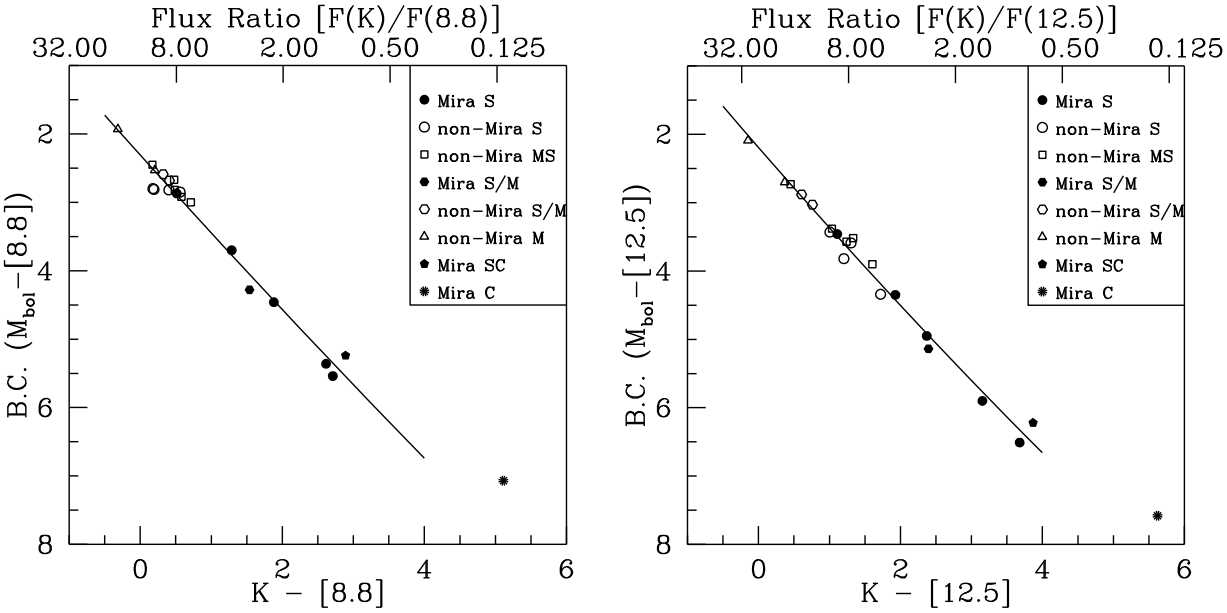

Fig. 3. Two examples of bolometric corrections, suitable for MS-S Stars with infrared photometry available. Correlation coefficients for the two relations are $R^2 = 0.98$ (*left*) and $R^2 = 0.99$ (*right*). Here and elsewhere "*K*" is a compact notation for the 2MASS filter K_s (*K*-short).

At this point we need to underline a relevant characteristic of the data displayed in Fig. 3. The corrections there used to infer the bolometric emission are applied to mid-infrared magnitudes, i.e. to data that, for our S stars with moderate IR excess, are essentially constant. This constancy of the mid-IR emission is important for estimating better bolometric corrections and is not shared by very red objects, e.g., by the carbon-rich Miras, where also the emission from the circumstellar envelope varies significantly in time (see Paper II). Anyhow, for our sample stars in Fig. 3 we expect roughly constant magnitudes at 8.8 or 12.5 μm, while the *K*(short) estimates from 2MASS, being single-epoch measurements, are affected by the photospheric variability (that can be up to 1−1.5 mag in near-IR). Different stars were certainly (randomly) sampled by 2MASS in different epochs of their light curves, but despite this, all the data fit a single regression line quite well. This can be so only if, during a cycle, the representative points of our stars move along the regression line itself. One might wonder why. The variability of AGB stars is not necessarily related only to a transfer of energy from one wavelength range to another (due to the star becoming cooler and more extended or hotter and more compact). There might be actually a global variability of the bolometric

magnitude itself, because we can see the addition, with different percent weight, of energy from finite-amplitude mechanical oscillations and shock waves affecting the envelope. The color dependence of these emissions is unknown to us, but we know experimentally that it does not extend to mid-IR for moderately red objects. If the chosen mid-IR magnitudes remain essentially constant, then bolometric corrections variable in time will be needed to compensate for the near-IR (and for the possible bolometric) variability. When the star is brighter it will require a larger correction, when it is dimmer the correction will be smaller, but as long as the regression line remains valid, the given formula for the B.C. should continue to hold. This would not be true if we had chosen, in the ordinate, a near-IR magnitude, still affected by the photospheric variability, having an unknown color dependence.

It remains however true the bolometric magnitudes given here, although possibly rather well estimated thanks to the use of mid-IR data, might be intrinsically variable. We have estimated how much the rather common variability by about 1 mag in K_s would affect the global flux, and this can reach up to 25% of the total. When estimating absolute bolometric magnitudes, throughout this paper, we apply both the corrections of Fig. 3 whenever possible, and then take the average of the absolute magnitudes thus obtained (the values to be averaged are in any case very close to each other).

We then applied the above corrections to the IR colors of sub-sample *B*, thus deriving also for them an estimate of the absolute bolometric magnitude. The input data and the derived parameters for this sample are shown in Tables 4 to 6.

A somewhat inverse procedure is applied to the sources of sample *C*, where luminosities can be inferred from period-luminosity relations. Here a comparison with the apparent bolometric magnitude, derived from bolometric corrections, yields the distance of the object. The recent updates in period-luminosity relations for AGB stars, which now allow for this possibility, are discussed in Appendix A.

The input data and the derived parameters for sample *C* are illustrated in Tables 7 to 9. The whole (more sparse) information we could compile for the bigger but so far incomplete sub-sample *D* is included instead in Tables 11 and 12, which we publish in electronic form at the CDS due to their dimensions. For the content of Table 10 see next section.

4. HR diagrams and luminosity functions

Using the IR fluxes collected in the previous section, and the information acquired on the absolute luminosities (see also Appendix A), we can now study the photometric properties of S stars and their relatives, with the aim of understanding how they are linked to the evolutionary status of the sources and to their chemical properties.

Figure 4 illustrates the $J - K$ vs. $K - [8.8]$ color–color diagram of the sources in our sample. The variability types appear rather well discriminated from IR colors. With only one exception (an SC star believed to be of Semiregular variability, but that we suspect is instead a misclassified Mira), all Semiregular and Irregular variables lay in the lower-left part of diagram, and remain separated by Miras by a dividing gap (the dashed line is just an eye's guide to illustrate this). Similarly, only very few objects classified as Miras fall at the left of the guiding line, all of them with short periods, while the vast majority is, in both colors, redder than Semiregulars and Irregulars. This is not surprising, in view of the fact that Miras are more efficient mass-losers and, as we argue below, are on average more evolved. We actually

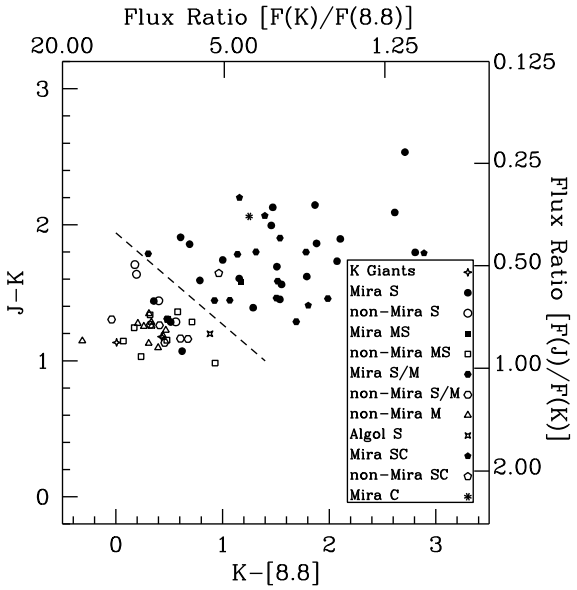

Fig. 4. A color–color diagram of the sources in samples *A* to *C*. All of them belong to the Stephenson's list, but some are misclassified: indeed, we find a few K and M giants, and a couple of C stars. Mira variables are redder than other sources in both colors and generally well separated from the rest by IR color criteria.

interpret the emerging evidence (from both the present sample and those of Papers I and II) as a suggestion that efficient radiation pressure on dust grains, powering fast mass lost, starts when the star has reached the Mira-like variability at periods in excess of about 200–230 days. In any case, the use of IR colors for discriminating different sources is interesting because the separation of the types is quite good, to the point that the IR colors might be used for guessing the variability type. (For example, if one picks up an AGB star of unknown variability, with $J - K$ and $K - [8.8]$ colors near 2, then we can reliably assume that it must be a Mira star.)

Figures 5 and 6 show two examples of the absolute H-R diagrams derived from our sample stars (the figures refer to both intrinsic and extrinsic sources). They are presented as a function of $J - K$ and $K - [8.8]$ colors, which can be considered as monitors either of the photosphere alone ($J - K$) or of the inner circumstellar environment ($K - [8.8]$). The link between fluxes in Jy and magnitudes in the various filters, hence to colors, is established by i) the distance correction (no extinction is assumed): and ii) the calibration of zero-magnitude fluxes given above.

The HR diagrams contain a large number of useful pieces of information on S star morphology and physics. We identify here a few such issues.

– Absolute magnitudes of Semiregular and Irregular variables stay on an almost vertical sequence, close to the region covered by AGB stellar models, albeit with remarkable scatter. Below this sequence, at the bottom of the plot, we find sources whose luminosities suggest that they are in an evolutionary stage preceding the thermally-pulsing AGB. These must necessarily be extrinsic S or MS stars; indeed, in most cases their extrinsic nature is already well established. For those sources (five) in this group for which no information on binarity is available, we suggest here, as a result of our luminosity calibration, that they are extrinsic and not yet on the TP-AGB (see the relative indication in bold and underlined in Tables 3, 6, 9). This suggestion will now need independent confirmations, which would also indirectly verify

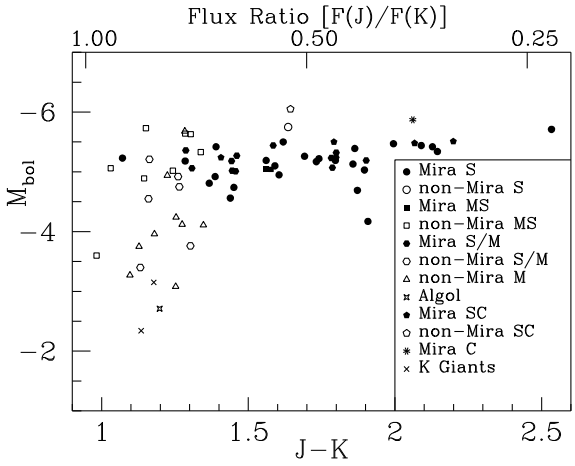

Fig. 5. An example of an absolute HR diagram, built using a near IR color index as abscissa.

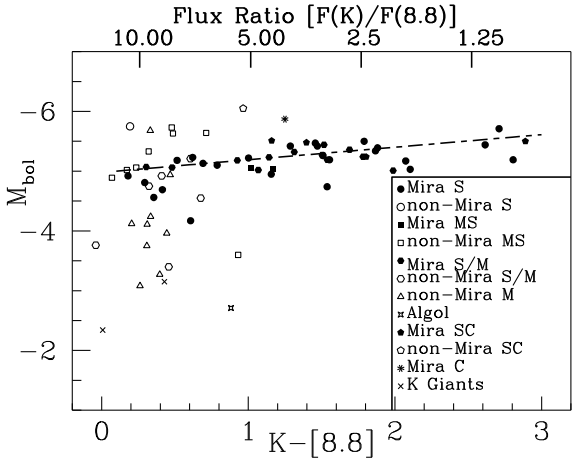

Fig. 6. An example of an absolute HR diagram, built using a near-to-mid IR color index as abscissa.

(or deny!) the validity of our bolometric corrections. If we are right, then extrinsic S stars should be the O-rich equivalent of the carbon rich R stars; Fig. 5 supports this guess in showing that lower-luminosity S stars are also warmer than the others.

– S-star infrared colors are different from those of C stars, being on average much bluer. Infrared excesses are less extreme, although mid-infrared (especially the [8.8] filter) remains the crucial wavelength range for understanding their physics: in particular we underline that, also for S stars, the best relations determining bolometric corrections are obtained by making use of mid-infrared colors.
– The un-reddened MS-S sources distributed along the vertical branch in Figs. 5 and 6 are more compatible with the evolutionary AGB tracks than for similarly-positioned C stars. Red-shifts of the track, requiring temperature corrections (and indicating inadequacy in molecular opacities of the envelope), although present, are largely reduced (by 0.5−1 mag) as compared to C stars (see Paper II).
– Absolute magnitudes of Mira variables are distributed over a relatively well defined distribution. They show a linear trend, indicating higher luminosities for redder colors and the correlation is clear, although the slope is small. In Fig. 6 we have added a least square curve based only on bona-fide, intrinsic S Miras. The relation is:

$$M_{\rm bol} = -0.2104 \cdot (K - [8.8]) - 4.9765 \quad (5)$$

with a correlation coefficient $R = 0.78$. Of course one expects different luminosities for sources of different colors (period-luminosity relations are such that the LPVs of longer period are also redder). It is however interesting to notice that, despite the infrared excesses increasingly separate the observed points from the AGB model tracks, we can nevertheless determine a systematic trend in the magnitude (now dominated by the circumstellar envelope). Moreover, it's remarkable that the correlation is sufficiently tight not to be confused by the observational errors.
If one computes a global average of the absolute magnitudes of Miras, this turns out to be -5.15 ± 0.4. Once stars have reached this luminosity range and are in the Mira variability stripe, further remarkable increases of luminosity seem to be no longer possible. This limiting range of luminosities (less than 1 mag wide) is close to a similar one that can be inferred for C-rich Miras in the data of Paper I. Since the range is relatively small, Mira variables appear to have, on average, similar Magnitudes, independent of the chemical composition of the atmosphere.
– We can confirm for S stars what was already said for C-stars: the Mira variability type tends to occur primarily at the end of the evolution. It was argued in the past that Semiregulars might be AGB stars in the low-luminosity post-flash dip (Kerschbaum & Hron 1996), so that a repeated transition between the two main variability types was expected. We cannot exclude this in general, but the high statistical relevance of Semiregular variables (almost as abundant as Miras in our global database, including sources of group *D*) cannot be explained by the post-flash phases, which, for advanced thermal pulses, occupy at most 25% of the TP-AGB duration (see also Fig. 8).
– The limited spread of Mira absolute magnitudes and the sufficiently good correlation with IR colors offer a tool for obtaining a first-order approximation to the luminosity and distance of Mira stars for which we do not have information beyond the measured colors. Indeed, for them one can first derive the apparent bolometric magnitude from our bolometric corrections; then one can assume, as a reasonable guess, that bolometric absolute magnitudes have an average of -5.15 ± 0.4 and a correlation with the $K - [8.8]$ color like the one shown for Fig. 6. This allows a determination of the distance from the distance modulus. An example of the application of this procedure to Mira variables in sample *D* is shown in Table 10.
– Stars differently classified along the sequence MS, S, SC show a different behavior also for what concerns the variability. Albeit with some scatter, one can notice that the MS classification is in general (with two possible exceptions) accompanied by the Semiregular or Irregular variability types, while a much larger percentage (about 60%) of S stars shows the Mira-type variability. Concerning SC stars, of the 5 objects for which we have detailed information, 4 are of Mira type; from the color−color diagram of Fig. 4 we suspect this should be so also for the fifth member, for which we suggest that the previous classification as a Semiregular might be wrong. SC stars are in general red, cool and luminous, like most S Miras. They might be the final evolutionary status of stars whose mass is barely sufficient to dredge-up enough carbon to approach unity in the C/O ratio.

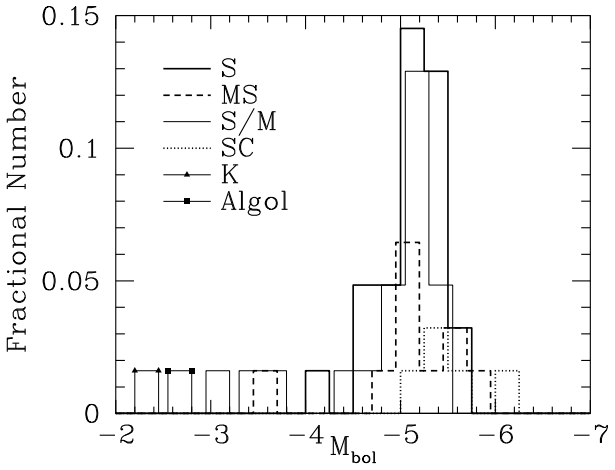

Fig. 7. The luminosity function of the stars in our samples *A* to *C*. Low luminosity sources are always extrinsic and the S stars define a very narrow distribution, characterized by a magnitude −5.15 ± 0.4.

The luminosity properties illustrated by the HR diagrams, and in particular the narrow range over which the magnitudes of MS-S Miras are distributed, are illustrated by the histogram of Fig. 7, showing the luminosity function of our sources. The distribution has a very well defined peak: all MS, S, SC stars lay in the range −4 to −6 and Mira S stars occupy a thin slice across the magnitude values −4.8 to −5.5. All the data points significantly far from this peak refer to extrinsic sources not belonging to the TP-AGB phase. Many (most) sources of uncertain classification (so far indicated as S/M) fall in the fiducial interval of the "best" S stars. We are pretty sure they are indeed S stars and probably Miras. In Tables 3, 6, 9 and 12 we indicate the possible classification deduced from Van Eck et al. (2000); Yang et al. (2006). In a few cases of discordant indications we prefer the physical analysis by Van Eck et al. (2000) and we show the other in parenthesis. For five sources in Tables 6 and 9, for which neither study offers a suggestion, we can infer that they are extrinsic from their low intrinsic luminosity.

Like for C stars, and actually even more so, the luminosities of Population I S stars are well defined inside a narrow range and are high enough that normal stellar models based on the Schwarzschild criterion for convection can adequately explain their formation. Once again, and as already noticed in Paper I, stellar models using large convective overshoot to favor dredge-up, and to obtain S-star and C-star chemical peculiarities at low luminosities (Izzard et al. 2007) appear to be unjustified, at least as far as the AGB evolutionary stages are concerned. Recently Bonačić Marinović et al. (2007) suggested that such models should be preferred for their capability of reproducing *s*-process abundances in stellar populations. One has however to mention that, from a theoretical point of view, the several free parameters still involved in any modelling probably make any conclusion provisional, and require observational verifications. Infrared observations, as presented here, do not confirm the need for large overshooting, at least for what concerns the ensuing stellar luminosities.

5. Conclusions

In this paper we have presented a reanalysis of the properties of MS-S-SC stars, based on a sample of about 600 sources, whose infrared fluxes from 1.25 to 21 μm were measured by the 2MASS, IRAS, ISO and MSX experiments. A "best" group of 21 stars (for which detailed ISO-SWS spectra are available up to long wavelengths) allowed us to obtain the bolometric magnitudes from an effective integral of the spectral energy distribution up to 45 μm. Correlations with near-to-mid IR colors then allowed us to infer bolometric corrections suitable to be applied to other groups of sources, with a less detailed coverage of the energy distribution. We can thus estimate with sufficient accuracy the apparent bolometric magnitudes of more than 500 sources. The whole analysis was performed in the photometric system suggested in Busso et al. (1996) and subsequently used in Papers I and II.

Criteria for obtaining the distance have then been discussed, from the simple use of revised astrometric measurements to a reformulation of the known period-luminosity relations for O-rich long period variables. The results of our analysis suggest that Mira variables of the S type have on average magnitudes in the range −5.15 ± 0.4, showing a well-defined linear correlation with infrared colors, especially the $K - [8.8]$ one. Low-mass AGB stars do not appear to proceed beyond the upper limit of the Mira luminosity range. Inside this range $P - L$ relations have become rather tight and accurate; they now form a very useful tool for determining intrinsic stellar parameters. From the $P - L$ relations and the $M_{\rm bol} - (K - [8.8])$ relation of Eq. (5) we now have tools to estimate the absolute magnitudes, hence the distances, of Mira S variables for which either the period or the infrared colors have been determined.

From statistical considerations it is also argued that Mira variables should occupy mainly the final part of the AGB track, as the simple intermittency between low-luminosity post flash dips and high-luminosity H-shell-powered stages is not sufficient to explain the available numbers of Semiregulars and Miras.

Luminosity functions confirm that intrinsic S stars (especially if in the Mira class) are distributed over a narrow range around the above average magnitude, and that this last datum is very close to the one previously found for C-stars. This is so to the point that it appears unlikely that a single AGB star can follow the whole M-MS-S-SC-C sequence, by simply increasing gradually its content of carbon and heavy elements as time passes, new dredge-up episodes enrich the envelope and the luminosity increases. Most probably, small differences in the initial mass and metallicity, almost indistinguishable once on the AGB, determine the final chemical fate of a star, which, for increasing initial mass, can end its life either as a MS-S giant, or a SC giant, or reaching effectively the C(N) stage. As an example of the effects of small mass (and metallicity) differences, Fig. 8 shows two AGB luminosity sequences obtained from the FRANEC code by Busso et al. (2003). The model star of the left panel does not reach the C-star phase, ending as an MS/S star. The evolutionary phases during which S-type chemical peculiarities are exhibited by the envelope are shaded in the plot. In the right panel we instead show the results of a model producing a real C-star: it has a slightly higher mass. Given the magnitudes we found in this paper for the sources of types MS and S, and those found in Paper I for C stars, most of the objects in our sample should belong to the mass and metallicity range covered by Fig. 8. If we broadly consider the typical magnitudes of S and C stars as being in the range −5.2 ± 0.4, then it is clear that this range includes both the S-star phase in the first panel of Fig. 8 and the S- and C-star phases in the right panel. It would be very difficult or impossible to distinguish between the two cases on the basis of their magnitudes, given the remaining uncertainties on distances and on possibly variable bolometric magnitudes.

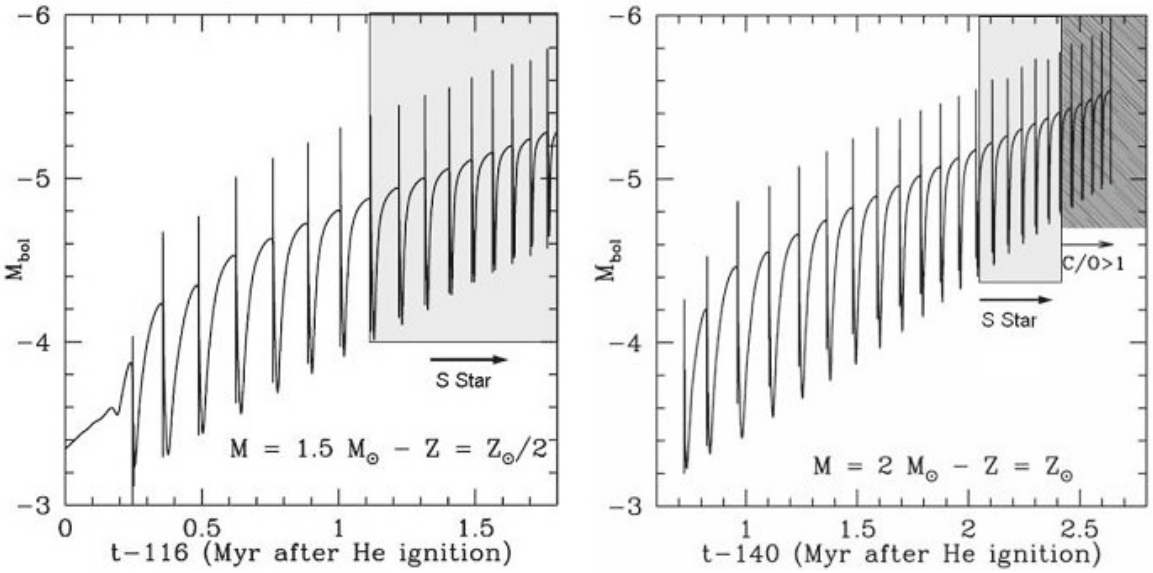

Fig. 8. The magnitude variations of two model stars of Population I, during the thermally pulsing AGB phase, as computed by the FRANEC code. The abscissa shows the time passed after the ignition of He-burning in the core, in Million years (once an offset is deduced, whose value is indicated). Most sources with features typical of S or C stars and magnitudes in the range -5.2 ± 0.4 should belong to the mass and metallicity range illustrated here, but only the star in the right panel does achieve the C/O > 1 condition.

The above results, and the typical initial mass implied for S and C stars (1.5−2 $M_{\odot}$) might appear rather peculiar, in view of the fact that about half of Planetary Nebulae are carbon rich. This cannot be explained by progenitors of around 2 $M_{\odot}$, at least according to the most common choices for the Initial Mass Function. However we must remember that the efficiency of dredge up strongly increases with decreasing metallicity. In halo stars one solar mass might be sufficient for forming a C star (also because the abundance of oxygen is very small). Hence the results presented here should be considered as valid only for galactic disc stars, at relatively high metallicities.

Acknowledgements. We are grateful to the anonymous referee for a very useful, careful and stimulating report, which greatly helped in the improvement of this work. We acknowledge support from the Italian Ministry of Research, under contract PRIN2006-022731, and from the section of Perugia of the National Institute for Nuclear Physics (INFN). This study is also part of the preparatory work for the IRAIT Antarctic telescope, of the Piano Nazionale delle Ricerche in Antartide (PNRA). These studies on Antarctic Astronomy are profiting of the financial support and cultural possibilities offered by the European Coordinating Action ARENA (within the FP6 plan). This research has made use of the SIMBAD database and the VizieR service (CDS, Strasbourg, France), and the IRSA (NASA/IPAC InfraRed Science Archive) database (USA), and the Astrogrid database (UK). In particular archived data from the experiments MSX, ISO-SWS and 2MASS were used. • The processing of the science data of the Midcourse Space eXperiment (MSX) was funded by the US Ballistic Missile Defense Organization with additional support from NASA Office of Space Science. • The Infrared Space Observatory (ISO) is an ESA project with instruments funded by ESA Member States (especially the PI countries: France, Germany, The Netherlands and UK). • 2MASS (Two Micron All Sky Survey) is a joint project of the Univ. of Massachusetts and the Infrared Processing and Analysis Center (IPAC) at California Institute of Technology, funded by NASA and the NSF (USA).

Appendix A: Period–luminosity relation

Mira stars have been alternatively suggested to be radially pulsating either in the fundamental mode, or in the first overtone (Tuchman 1999; Feast 1999). For Semiregular variables various overtones and the same fundamental mode are also possible. The discussion on these properties has gone on for three decades, although the large database made available by the MACHO project (Alcock et al. 1992) seems to favor the fundamental mode for Miras (Wood et al. 1999).

The non-unique pulsational properties of Semiregular variables imply that there is not a unique $P - L$ relation for them (Bedding & Zijlstra 1998). Instead, such relations for O-rich and C-rich Miras have become increasingly accurate and statistically relevant, to the point of forming now an invaluable tool in the difficult task of determining the distances of Long Period Variables. Many studies in the past were dedicated to correlate $LogP$ with magnitudes obtained in the K filter (Feast et al. 1989; Hughes & Wood 1990; Wood & Sebo 1996). This method, however, meets the difficulty of the still remarkable light-curve amplitude at 2 μm. Relations directly connecting the period to the bolometric magnitude (Feast et al. 1989; Whitelock et al. 1994, 2006) are therefore precious, although obviously more difficult to obtain.

Different relations are expected (and found) for C-rich and O-rich objects (see in particular Whitelock & Feast 2000; Whitelock et al. 2006). For our sample of S-stars, which have C/O ≤ 1, we can use the $M_{\rm bol} - P$ relation suggested for O-rich Miras by Feast et al. (1989) and Whitelock et al. (1994).

Another formula, established for Magellanic Cloud O-rich Miras, but suitable also for the Galaxy in view of the universality of the slope (Feast 2004), was presented recently by Whitelock et al. (2008). This last relation is based on the K-magnitude. It is difficult to establish criteria for choosing between the two, so that we decided to use both, and then take an average of the results. (We underline that both the original relations were derived for O-rich sources and should therefore apply also to S stars, where the ratio C/O does not reach unity.) In particular, our procedure was the following one. i) We firstly derived apparent bolometric magnitudes from the bolometric corrections of Fig. 3, then we applied the relations by Whitelock et al. (1994) to obtain an estimate of the absolute bolometric magnitudes. Hence from the distance modulus we could infer a first value for the distance. ii) Separately, we applied the formula by Whitelock et al. (2008) to derive the absolute K magnitude, then by comparison with the 2MASS measurement we deduced a second estimate for the

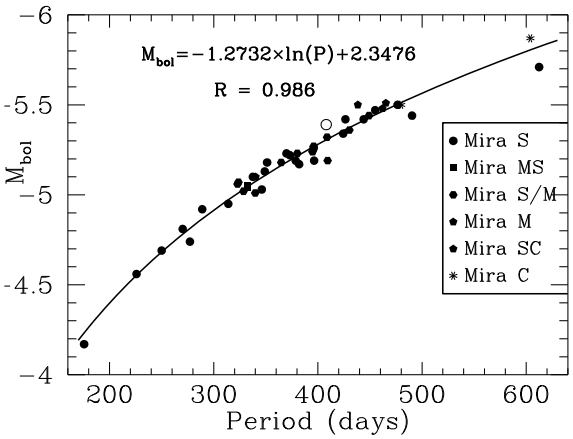

Fig. A.1. The average period–luminosity relation deduced for Miras (filled symbols). The open circle refers to χ Cyg, whose magnitude, deduced independently from its IR fluxes, its bolometric correction and its Hipparcos distance, fits well in the general relation. The curve represents the written fitting relation, and R is its regression coefficient. See text for further explanations.

distance. The two distance values were then averaged to get a final choice. This choice for the stellar distance was then applied to our apparent bolometric magnitudes, thus deducing our best estimate for the absolute bolometric Magnitude.

Although certainly intricate, the above procedure should minimize the systematic errors of each individual method. The absolute magnitudes thus deduced are plotted as a function of the period in Fig. A.1, thus providing our choice for the *average* $P-L$ relation, descending primarily from the quoted works, but also from our averaging technique and from our estimate of the bolometric corrections. The derived period–magnitude relation can be expressed by a fitting spline with a high accuracy, as shown on the same graph. In the plot, we also included, as a comparison, a point (the open circle) corresponding to the Mira star χ *Cyg*. For it we did not apply any $P-L$ relation: the absolute magnitude was obtained from directly scaling our apparent bolometric magnitude with the known Hipparcos distance (van Leeuwen 2007a). Although it's only a single point, its good accord with the trend defined by the other sources gives us a consistency check for the technique.

References

Alcock, C., Axelrod, T. S., Bennett, D. P., et al. 1992, Robotic telescopes in the 1990s, 103rd Annual Meeting of the ASP, Univ. of Wyoming, Laramie, 1991, 193
Allende Prieto, C., Lambert, D. L., & Asplund, M. 2002, ApJ, 573, L137
Anders, E., & Grevesse, N. 1989, Geochem. Cosmochem. Acta, 53, 197
Andersen, A. C., Höfner, S., & Gautschy-Loidl, R. 2003, A&A, 400, 981
Bedding, T. R., & Zijlstra, A. A. 1998, ApJ, 506, L47
Bessell, M. S., Castelli, F., & Plez, B. 1998, A&A, 333, 231
Bonačić Marinović, A., Izzard, R. G., Lugaro, M., & Pols, O. R. 2007, A&A, 469, 1013
Busso, M., Gallino, R., Lambert, D. L., Raiteri, C. M., & Smith, V. V. 1992, ApJ, 399, 218
Busso, M., Lambert, D. L., Beglio, L., et al. 1995, ApJ, 446, 775
Busso, M., Origlia, L., Marengo, M., et al. 1996, A&A, 311, 253
Busso, M., Gallino, R., & Wasserburg, G. J. 1999, ARA&A, 37, 239
Busso, M., Gallino, R., Lambert, D. L., Travaglio, C., & Smith, V. V. 2001, ApJ, 557, 802
Busso, M., Gallino, R., & Wasserburg, G. J. 2003, PASA, 20, 356
Busso, M., Guandalini, R., Persi, P., Corcione, L., & Ferrari-Toniolo, M. 2007, AJ, 133, 2310 (Paper II)
Carciofi, A. C., Bjorkman, J. E., & Magalhães, A. M. 2004, ApJ, 604, 238
Cioni, M.-R. L., Blommaert, J. A. D. L., Groenewegen, M. A. T., et al. 2003, A&A, 406, 51
Cohen, J. G., Persson, S. E., Elias, J. H., & Frogel, J. A. 1981, ApJ, 249, 481
Cohen, M., Wheaton, Wm. A., & Megeath, S. T. 2003, AJ, 126, 1090
Cutri, R. M., Skrutskie, M. F., van Dyk, S., et al. 2003, VizieR On-line Data Catalog: II/246, University of Massachusetts and Infrared Processing and Analysis Center (IPAC/California Institute of Technology)
Feast, M. 1999, IAUS, 191, 109
Feast, M. 2004, IAU Colloq., 193, Proceedings of the conference held 6−11 July, 2003 at Christchurch, New Zealand, ed. D. W. Kurtz, & K. R. Pollard (San Francisco: ASP), ASP Conf. Proc., 310, 304
Feast, M. W., Glass, I. S., Whitelock, P. A., & Catchpole, R. M. 1989, MNRAS, 241, 375
Glass, I. S. 1999, The Handbook of Infrared Astronomy (Cambridge, England: Cambridge University Press)
Groenewegen, M. A. T., Sevenster, M., Spoon, H. W. W., & Pérez, I. 2002, A&A, 390, 511
Guandalini, R., Busso, M., Ciprini, S., Silvestro, G., & Persi, P. 2006, A&A, 445, 1069 (Paper I)
Habing, H. J. 1996, A&ARv, 7, 97
Hughes, S. M. G., & Wood, P. R. 1990, AJ, 99, 784
Izzard, R. G., Jeffery, C. S., & Lattanzio, J. C. 2007, A&A, 470, 661
Kerschbaum, F., & Hron, J. 1996, A&A, 308, 489
Knapp, G. R., & Morris, M. 1985, ApJ, 292, 640
Le Bertre, T., Matsuura, M., Winters, J. M., et al. 2001, A&A, 376, 997
Le Bertre, T., Tanaka, M., Yamamura, I., & Murakami, H. 2003, A&A, 403, 943
Marigo, P., Girardi, L., & Chiosi, C. 2003, A&A, 403, 225
Merrill, S. P. W. 1952, ApJ, 116, 21
Olivier, E. A., & Wood, P. R. 2003, ApJ, 584, 1035
Olofsson, A. O. H., Olofsson, G., Hjalmarson, Å., et al. 2003, A&A, 402, 47
Omont, A., Gilmore, G. F., Alard, C., et al. 2003, A&A, 403, 975
Salpeter, E. E. 1974, ApJ, 193, 585
Samus, N. N., Durlevich, O. V., et al. 2004, VizieR On-line Data Catalog: II/250, Institute of Astronomy of Russian Academy of Science and Sternberg, State Astronomical Institute of the Moscow State University
Sandin, C., & Höfner, S. 2003a, A&A, 398, 253
Sandin, C., & Höfner, S. 2003b, A&A, 404, 789
Sedlmayr, E. 1994, Lecture Notes in Physics, 428, 163
Smith, V. V., & Lambert, D. L. 1986, ApJ, 311, 843
Smith, V. V., & Lambert, D. L. 1990, ApJS, 72, 387
Stephenson, C. B. 1984, A General Catalogue of Galactic S-Stars, edn.2 (Warner & Swasey Observatory)
Stephenson, C. B. 1990, AJ, 100, 569
Tuchman, Y. 1999, IAUS, 191, 123
Uttenthaler, S., Hron, J., Lebzelter, T., et al. 2007, A&A, 463, 251
Van Eck, S., Jorissen, A., Udry, S., et al. 2000, A&AS, 145, 51
van Leeuwen, F. 2007a, Hipparcos: The new reduction of the raw data (Berlin: Springer)
van Leeuwen, F. 2007b, A&A, 474, 653
Wachter, A., Schröder, K.-P., Winters, J. M., Arndt, T. U., & Sedlmayr, E. 2002, A&A, 384, 452
Whitelock, P., & Feast, M. 2000, MNRAS, 319, 759
Whitelock, P., Menzies, J., Feast, M., et al. 1994, MNRAS, 267, 711
Whitelock, P. A., Feast, M. W., Marang, F., & Groenewegen, M. A. T. 2006, MNRAS, 369, 751
Whitelock, P. A., Feast, M. W., & van Leeuwen, F. 2008, MNRAS, Online Early, 393
Winters J. M., Le Bertre, T., Jeong, K. S., Nyman, L.-Å., & Epchtein, N. 2003, A&A, 409, 715
Wood, P. R. 2003, Mass-losing pulsating stars and their circumstellar matter, Workshop, May 13−16, 2002, Sendai, Japan, ed. Y. Nakada, M. Honma, & M. Seki (Dordrecht: Kluwer Academic Publishers), Astrophys. Space Sci. Library, 283, 3
Wood, P. R., & Cohen, M. 2001, Post-AGB Objects as a Phase of Stellar Evolution, Proceedings of the Torun Workshop held July 5−7, 2000, ed. R. Szczerba, & S. K. Górny (Kluwer Academic Publishers), Astrophys. Space Sci. Library, 265, 71
Wood, P. R., & Sebo, K. M. 1996, MNRAS, 282, 958
Wood, P. R., Alcock, C., Allsman, R. A., et al. 1999, IAUS, 191, 151
Wood, P. R., Olivier, E. A., & Kawaler, S. D. 2004, ApJ, 604, 800
Yang, X., Chen, P., Wang, J., & He, J. 2006, AJ, 132, 1468
Zijlstra, A. A., Bedding, T. R., Markwick, A. J., et al. 2004, MNRAS, 352, 325
Zinner, E. 2000, Meteoritics & Planetary Science, 35, Supplement, A177

Table 1. Sample *A* − first part. Spectral type is from the GCVS catalogue whenever possible, otherwise it is obtained from the SIMBAD Astronomical Database.

IRAS name	Other name	Stephenson name	Coordinates ICRS	Spectral type	Var. type (GCVS)
01159+7220	S Cas	CSS 28	01 19 41.97 +72 36 39.3	S3,4e−S5,8e	M
19126−0708	W Aql	CSS 1115	19 15 23.44 −07 02 49.9	S3,9e−S6,9e	M
19354+5005	R Cyg	CSS 1150	19 36 49.381 +50 11 59.46	S2.5,9e−S6,9e(Tc)	M
19486+3247	chi Cyg	CSS 1165	19 50 33.9220 +32 54 50.610	S6,2e−S10,4e/MSe	M
23595−1457	W Cet	CSS 1346	00 02 07.3891 −14 40 33.065	S6,3e−S9,2e	M
22196−4612	pi1 Gru	CSS 1294	22 22 44.2053 −45 56 52.598	S5,7e	SRB
20026+3640	AA Cyg	CSS 1188	20 04 27.6055 +36 49 00.465	S7,5−S7.5,6(MpTc)	SRB
20120−4433	RZ Sgr	CSS 1196	20 15 28.4049 −44 24 37.480	S4,4ep	SRB
03452+5301	WX Cam	CSS 82	03 49 03.77 +53 10 59.2	S5,8	LB
23070+0824	GZ Peg	CSS 1322	23 09 31.4570 +08 40 37.778	M4SIII	SRA
15492+4837	ST Her	CSS 903	15 50 46.6248 +48 28 58.856	M6−7IIIaS	SRB
00192−2020	T Cet	CSS 8	00 21 46.2737 −20 03 28.885	M5−6SIIe	SRC
05374+3153	NO Aur	CSS 149	05 40 42.0504 +31 55 14.187	M2SIab	LC
22476+4047	RX Lac	CSS 1308	22 49 56.8992 +41 03 04.312	M7.5Se	SRB
00213+3817	R And	CSS 9	00 24 01.9469 +38 34 37.328	S3,5e−S8,8e/M7e	M
22521+1640	HR Peg	CSS 1315	22 54 35.6272 +16 56 30.601	S5,1/M4	SRB
17553+4521	OP Her	–	17 56 48.5274 +45 21 03.063	M5IIb−IIIa/S	SRB
13372−7136	LY Mus	CSS 826	13 41 13.5883 −71 52 05.767	M4III	LB
18058−3658	–	CSS 1023	18 09 17.1853 −36 57 57.614	M2II−III	–
19111+2555	S Lyr	CSS 1112	19 13 11.79 +26 00 28.3	SCe	M
15194−5115	II Lup	CSS 886	15 23 04.91 −51 25 59.0	C	M

Table 2. Sample *A* − second part.

Source name	*J* [Jy]	*H* [Jy]	*K* [Jy]	[8.8] [Jy]	[9.8] [Jy]	[11.7] [Jy]	[12.5] [Jy]	*D* [Jy]	*E* [Jy]	Mid−IR Data Origin	ISO TDT number
S Cas	56.6	168	244	232	316	304	281	235	185	ISO−SWS1	41602133
W Aql	388	822	1113	969	1099	1043	789	625	488	ISO−SWS1	16402335
R Cyg	200	288	302	77.3	87.8	79.3	69.2	52.8	29.7	ISO−SWS1	42201625
chi Cyg	1365	2823	3176	1408	1655	1579	1095	736	487	ISO−SWS1	15900437
W Cet	74.1	113	101	12.7	12.4	10.5	10.9	8.3	4.5	ISO−SWS1	37802225
pi1 Gru	3080	–	5812	544	632	679	683	505	365	ISO−SWS1	34402039
AA Cyg	238	389	375	42.6	42.5	42.9	36.8	27.5	16.9	ISO−SWS1	36401817
RZ Sgr	139	206	190	25.0	26.2	25.7	24.5	21.8	21.0	ISO−SWS1	14100818
WX Cam	43.5	79.3	87.6	8.1	7.9	8.4	16.6	9.3	4.0	ISO−SWS1	81002721
GZ Peg	735	1100	965	88.6	78.9	62.4	56.8	40.9	21.0	ISO−SWS1	37600306
ST Her	804	1162	1098	166	186	200	187	149	104	ISO−SWS1	41901305
T Cet	1009	1596	1403	172	163	172	171	134	83.0	ISO−SWS1	55502308 − 37801819
NO Aur	226	362	273	33.2	41.6	46.3	36.1	23.3	17.2	ISO−SWS1	86603434
RX Lac	465	737	681	91.0	85.4	81.9	68.6	50.3	28.8	ISO−SWS1	78200427
R And	247	506	596	193	264	248	210	176	135	ISO−SWS1	40201723
HR Peg	191	327	256	27.0	24.4	20.9	20.0	12.6	7.8	ISO−SWS1	37401910
OP Her	416	731	556	63.5	58.1	46.4	37.8	30.9	16.0	ISO−SWS1	77800625
LY Mus	221	334	300	28.4	24.7	19.7	16.4	12.9	7.6	ISO−SWS1	13201304
CSS 1023	33.2	51.7	39.9	2.3	2.2	1.5	1.4	0.83	0.46	ISO−SWS1	14100603
S Lyr	8.2	13.2	17.9	20.0	23.2	25.5	24.4	22.1	15.7	ISO−SWS1	52000546
II Lup	3.7	25.5	99.0	860	852	860	681	506	391	ISO−SWS6	29700401

Table 3. Sample *A* – third part. The indication I. – E. (Intrinsic – Extrinsic) is given according to the suggestions from Van Eck et al. (2000) and Yang et al. (2006). In discordant cases we prefer the choice by Van Eck et al. (2000) and show the one of Yang et al. (2006) in parenthesis. For few sources, for which neither study offers a suggestion, we infer that they are extrinsic from their low intrinsic luminosity: in the tables they are underlined.

Source name	Var. type (GCVS)	Period (GCVS)	Distance (kpc)	Min. – Max. (kpc)	Ref. distance	Bol. magnitudes ISO integration	I. – E.
S Cas	M	612.43	0.85	–	$P-L$ / this paper	−5.71	I
W Aql	M	490.43	0.34	–	$P-L$ / this paper	−5.44	I
R Cyg	M	426.45	0.55	–	$P-L$ / this paper	−5.42	–
chi Cyg	M	408.05	0.18	0.15 – 0.22	Hip. / van Leeuwen (2007a)	−5.39	I
W Cet	M	351.31	0.83	–	$P-L$ / this paper	−5.18	I
pi1 Gru	SRB	150	0.16	0.15 – 0.19	Hip. / van Leeuwen (2007a)	−5.75	I
AA Cyg	SRB	212.7	–	–	–	–	I
RZ Sgr	SRB	223.2	–	–	–	–	I
WX Cam	LB	–	–	–	–	–	I
GZ Peg	SRA	92.66	0.24	0.22 – 0.26	Hip. / van Leeuwen (2007a)	−5.02	E
ST Her	SRB	148	0.30	0.25 – 0.36	Hip. / van Leeuwen (2007a)	−5.64	I
T Cet	SRC	158.9	0.27	0.24 – 0.31	Hip. / van Leeuwen (2007a)	−5.63	I
NO Aur	LC	–	0.60	0.47 – 0.83	Hip. / van Leeuwen (2007a)	−5.73	I
RX Lac	SRB	650	–	–	–	–	I
R And	M	409.33	0.41	–	$P-L$ / this paper	−5.19	I
HR Peg	SRB	50	0.41	0.36 – 0.50	Hip. / van Leeuwen (2007a)	−4.75	I
OP Her	SRB	120.5	0.30	0.27 – 0.32	Hip. / van Leeuwen (2007a)	−4.92	–
LY Mus	LB	–	0.29	0.26 – 0.33	Hip. / van Leeuwen (2007a)	−4.12	E
CSS 1023	–	–	–	–	–	–	E
S Lyr	M	438.4	2.27	–	$P-L$ / this paper	−5.50	I
II Lup	M	–	0.59	–	Groenewegen et al. (2002)	−4.82	–

Table 4. Sample *B* – first part. Suggestions from Smith & Lambert (1986) for Spectral Type: *1* RS Cnc: M6eIIIaS. *2* V1743 Cyg: M5IIIaS. *3* V1981 Cyg: M4IIIaS.

IRAS name	Other name	Stephenson name	Coordinates ICRS	Spectral type	Var. type (GCVS)
05199−0842	V1261 Ori	CSS 133	05 22 18.6453 −08 39 58.034	S	Algol type
04497+1410	omi Ori	CSS 114	04 52 31.9621 +14 15 02.311	M3.2IIIaS	SRB
10226+0902	DE Leo	–	10 25 15.1951 +08 47 05.441	M2IIIabS	SRB
07245+4605	Y Lyn	CSS 347	07 28 11.6109 +45 59 26.207	M6SIb−II	SRC
07392+1419	NZ Gem	CSS 382	07 42 03.2185 +14 12 30.612	M3II−IIIS	SR
06457+0535	V613 Mon	CSS 260	06 48 22.2963 +05 32 30.050	M2/S5,1	SRB
09076+3110	RS Cnc	CSS 589	09 10 38.7990 +30 57 47.300	M6eIb−II/S [1]	SRC
03377+6303	BD Cam	CSS 79	03 42 09.3250 +63 13 00.501	S5,3/M4III	LB
07095+6853	AA Cam	CSS 312	07 14 52.0703 +68 48 15.380	M5/S	LB
13079−8931	BQ Oct	CSS 804	14 35 29.5001 −89 46 18.182	M4III/S5,1	LB
12272−4127	V928 Cen	CSS 796	12 29 57.8871 −41 44 09.242	M2II−III	SRB
19323+4909	V1743 Cyg	–	19 33 41.6068 +49 15 44.347	M4.5III [2]	SRB
–	V1981 Cyg	–	21 02 24.1993 +44 47 27.528	M4s... [3]	SRB
08214−3807	V436 Pup	CSS 500	08 23 16.9344 −38 17 09.884	M1III	LB
–	V2141 Cyg	CSS 1254	20 57 53.1771 +44 47 17.336	M1	LB
12106−3350	V335 Hya	–	12 13 12.9423 −34 07 30.981	M4III	LB
14510−6052	CR Cir	CSS 867	14 54 56.9389 −61 04 33.027	M2/M3II	LC
16418−1359	–	CSS 937	16 44 42.1936 −14 04 48.553	M1III	–
13136−4426	UY Cen	CSS 816	13 16 31.8300 −44 42 15.741	SC	SR
16425−1902	–	CSS 938	16 45 30.1769 −19 08 12.939	K5II	–
20076+3331	–	CSS 1194	20 09 32.9873 +33 40 53.851	K5III	–

Table 5. Sample B – second part.

Source name	J [Jy]	H [Jy]	K [Jy]	[8.8] [Jy]	[9.8] [Jy]	[11.7] [Jy]	[12.5] [Jy]	D [Jy]	E [Jy]	Mid–IR data origin
V1261 Ori	73.8	111	93.1	16.4	16.5	19.6	21.3	–	–	IRAS–LRS
omi Ori	1022	1587	1227	103	82.4	64.8	60.9	–	–	IRAS–LRS
DE Leo	178	234	184	34.0	30.7	34.4	36.4	–	–	IRAS–LRS
Y Lyn	876	1448	1256	132	150	121	107	–	–	IRAS–LRS
NZ Gem	369	566	399	38.9	34.5	32.6	32.5	–	–	IRAS–LRS
V613 Mon	49.6	74.3	68.9	5.2	–	–	3.3	2.0	–	MSX
RS Cnc	3065	4324	3742	512	693	493	436	–	–	TIRCAM2
BD Cam	439	630	521	62.3	52.5	43.6	41.2	–	–	IRAS–LRS
AA Cam	146	220	185	–	–	–	–	–	–	–
BQ Oct	139	196	170	24.8	22.5	23.5	23.6	–	–	IRAS–LRS
V928 Cen	196	267	225	25.4	21.9	20.3	20.5	–	–	IRAS–LRS
V1743 Cyg	259	421	335	40.4	36.4	34.5	34.2	–	–	IRAS–LRS
V1981 Cyg	197	279	245	28.9	–	–	16.3	10.8	4.7	MSX
V436 Pup	139	198	165	17.1	–	–	10.3	7.0	2.7	MSX
V2141 Cyg	147	216	195	20.8	–	–	12.2	8.2	3.5	MSX
V335 Hya	611	946	833	88.6	78.7	67.4	63.3	–	–	IRAS–LRS
CR Cir	75.1	117	99.6	9.9	–	–	5.8	3.8	–	MSX
CSS 937	104	169	151	15.7	15.9	20.1	21.6	–	–	IRAS–LRS
UY Cen	184	360	350	66.7	62.9	61.4	55.6	–	–	IRAS–LRS
CSS 938	142	200	175	20.4	19.7	21.4	23.2	–	–	IRAS–LRS
CSS 1194	31.1	41.5	37.0	2.9	–	–	2.4	0.96	–	MSX

Table 6. Sample B – third part.

Source name	Var. type (GCVS)	Period (GCVS)	Distance (kpc)	Min. – Max. (kpc)	Ref. distance	Bol. magnitudes Bol. corrections	I. – E.
V1261 Ori	Algol Type	–	0.29	0.23 – 0.38	Hip. / van Leeuwen (2007a)	−2.71	E
omi Ori	SRB	30	0.20	0.17 – 0.23	Hip. / van Leeuwen (2007a)	−4.89	I
DE Leo	SRB	–	0.31	0.27 – 0.37	Hip. / van Leeuwen (2007a)	−3.60	*E*
Y Lyn	SRC	110	0.25	0.20 – 0.33	Hip. / van Leeuwen (2007a)	−5.33	I
NZ Gem	SR	–	0.39	0.32 – 0.51	Hip. / van Leeuwen (2007a)	−5.06	E
V613 Mon	SRB	–	0.50	0.35 – 0.84	Hip. / van Leeuwen (2007a)	−3.76	E
RS Cnc	SRC	120	0.14	0.13 – 0.15	Hip. / van Leeuwen (2007a)	−5.21	I
BD Cam	LB	–	0.16	0.15 – 0.17	Hip. / van Leeuwen (2007a)	−3.40	E
AA Cam	LB	–	0.78	0.50 – 1.82	Hip. / van Leeuwen (2007a)	–	I
BQ Oct	LB	–	0.49	0.41 – 0.60	Hip. / van Leeuwen (2007a)	−4.55	I
V928 Cen	SRB	–	0.23	0.21 – 0.25	Hip. / van Leeuwen (2007a)	−3.27	E
V1743 Cyg	SRB	40	0.41	0.38 – 0.44	Hip. / van Leeuwen (2007a)	−4.94	–
V1981 Cyg	SRB	–	0.30	0.27 – 0.33	Hip. / van Leeuwen (2007a)	−3.96	*E*
V436 Pup	LB	–	0.33	0.30 – 0.38	Hip. / van Leeuwen (2007a)	−3.75	E
V2141 Cyg	LB	–	0.38	0.31 – 0.51	Hip. / van Leeuwen (2007a)	−4.24	*E*
V335 Hya	LB	–	0.36	0.31 – 0.43	Hip. / van Leeuwen (2007a)	−5.68	–
CR Cir	LC	–	0.31	0.25 – 0.42	Hip. / van Leeuwen (2007a)	−3.08	E
CSS 937	–	–	0.42	0.31 – 0.66	Hip. / van Leeuwen (2007a)	−4.11	E
UY Cen	SR	114.6	0.69	0.47 – 1.33	Hip. / van Leeuwen (2007a)	−6.05	I
CSS 938	–	–	0.25	0.20 – 0.33	Hip. / van Leeuwen (2007a)	−3.15	E
CSS 1194	–	–	0.36	0.30 – 0.45	Hip. / van Leeuwen (2007a)	−2.34	*E*

Table 7. Sample C − first part.

IRAS name	Other name	Stephenson name	Coordinates ICRS	Spectral type	Var. type (GCVS)
04352+6602	T Cam	CSS 103	04 40 08.8768 +66 08 48.654	S4,7e−S8.5,8e	M
06571+5524	R Lyn	CSS 283	07 01 18.0093 +55 19 49.766	S2.5,5e−S6,8e:	M
07043+2246	R Gem	CSS 307	07 07 21.2744 +22 42 12.736	S2,9e−S8,9e(Tc)	M
07092+0735	WX CMi	CSS 316	07 11 57.45 +07 29 59.3	Se	M
12417+6121	S UMa	CSS 803	12 43 56.676 +61 05 35.51	S0,9e−S5,9e	M
15030−4116	GI Lup	CSS 872	15 06 16.31 −41 28 14.1	S7,8e	M
23554+5612	WY Cas	CSS 1345	23 58 01.30 +56 29 13.5	S6,5pe	M
00135+4644	X And	CSS 6	00 16 09.57 +47 00 44.8	S2,9e−S5,5e	M
00435+4758	U Cas	CSS 12	00 46 21.371 +48 14 38.72	S3,5e−S8,6e	M
06062+2830	GH Aur	CSS 191	06 09 27.71 +28 29 43.4	S	M
07197−1451	TT CMa	CSS 341	07 22 02.00 −14 56 56.7	S	M
07584−2051	EX Pup	CSS 443	08 00 38.31 −20 59 35.3	S2,4e	M
11179−6135	RY Car	CSS 742	11 20 11.39 −61 52 16.8	S7,8e	M
13226−6302	NZ Cen	CSS 820	13 26 02.52 −63 18 28.5	Se	M
14212+8403	R Cam	CSS 856	14 17 51.0439 +83 49 53.861	S2,8e−S8,7e	M
17478−2957	V762 Sgr	CSS 1001	17 51 04.04 −29 58 30.9	S6,4	M
17490−3502	V407 Sco	CSS 1004	17 52 25.53 −35 03 17.5	Se	M
19166+0318	ER Aql	CSS 1121	19 19 06.99 +03 24 05.2	S	M
23376+6304	V441 Cas	CSS 1338	23 39 58.92 +63 20 55.1	S	M
23489+6235	EO Cas	CSS 1342	23 51 27.30 +62 51 47.0	Se	M
00001+4826	IW Cas	CSS 1347	00 02 44.22 +48 42 50.9	S4.5,9e	M
–	–	CSS2 10	02 51 33.00 +57 50 34.5	S	M
10237−6135	AU Car	CSS 679	10 25 29.74 −61 50 59.1	MS	M
10349−6203	RX Car	CSS 690	10 36 45.82 −62 19 16.8	MS	M
02143+4404	W And	CSS 49	02 17 32.9606 +44 18 17.766	S6,1e−S9,2e/M4−M1	M
07149+0111	RR Mon	CSS 326	07 17 31.54 +01 05 41.5	S7,2e−S8,2e/M6−10	M
07545−4400	SU Pup	CSS 436	07 56 12.0813 −44 08 33.254	M/S4,2e	M
09338−5349	UU Vel	CSS 614	09 35 33.21 −54 03 25.9	M2e/S7,8e	M
17001−3651	RT Sco	CSS 954	17 03 32.56 −36 55 13.7	S7,2/M6e−M7e	M
20213+0047	V865 Aql	CSS 1211	20 23 54.6422 +00 56 44.794	M6−M7/S7,5e:	M
00445+3224	RW And	CSS 14	00 47 18.92 +32 41 08.6	M5e−M10e/S6,2e	M
07103−0258	AK Mon	CSS 319	07 12 49.91 −03 03 29.0	M5/S5,1	M
17521−2907	V745 Sgr	CSS 1007	17 55 19.00 −29 07 54.4	Se/M	M
20044+5750	S Cyg	CSS 1191	20 05 29.85 +57 59 09.1	S2.5,1e/M3.5−M7e	M
20369+3742	FF Cyg	CSS 1232	20 38 51.71 +37 53 23.2	S6,8e/M4e	M
03499+4730	FG Per	CSS 85	03 53 30.2 +47 39 04	M9	M
13163−6031	TT Cen	CSS 817	13 19 35.016 −60 46 46.26	CSe	M
18586−1249	ST Sgr	CSS 1096	19 01 29.20 −12 45 34.0	C4,3e−S9,5e	M
21540+4806	LX Cyg	CSS 1286	21 55 57.03 +48 20 52.6	SC3e−S5,5e:	M
18575−0139	VX Aql	CSS 1093	19 00 09.61 −01 34 56.8	C9,1p/M0ep	M
01097+6154	V418 Cas	CSS 23	01 12 59.89 +62 10 47.6	–	M

Table 8. Sample C − second part.

Source name	J [Jy]	H [Jy]	K [Jy]	[8.8] [Jy]	[9.8] [Jy]	[11.7] [Jy]	[12.5] [Jy]	D [Jy]	E [Jy]	Mid−IR data origin
T Cam	152	306	315	62.1	53.4	48.8	47.1	–	–	IRAS−LRS
R Lyn	51.7	77.7	91.1	29.9	29.9	29.2	28.5	–	–	IRAS−LRS
R Gem	155	226	174	24.1	–	–	21.4	16.3	7.5	MSX
WX CMi	8.9	13.8	17.3	8.3	–	–	9.2	6.3	4.1	MSX
S UMa	26.3	43.4	41.4	4.5	–	2.8	3.1	–	–	TIRCAM2
GI Lup	61.7	115	128	–	–	–	–	–	–	–
WY Cas	64.5	94.4	120	48.8	55.6	58.2	55.0	–	–	IRAS−LRS
X And	18.1	37.3	43.3	23.6	23.6	24.9	26.6	–	–	IRAS−LRS
U Cas	29.6	45.0	47.1	15.2	15.6	19.4	20.3	–	–	IRAS−LRS
GH Aur	4.4	7.8	10.2	1.5	–	–	1.8	–	–	MSX
TT CMa	29.6	50.1	54.3	12.3	–	–	14.1	10.8	7.7	MSX
EX Pup	3.9	5.9	5.8	0.54	–	–	–	–	–	MSX
RY Car	8.3	18.2	25.1	11.0	–	–	8.9	5.6	3.2	MSX
NZ Cen	8.3	15.7	17.2	9.1	–	–	9.3	6.3	5.2	MSX
R Cam	47.2	70.8	69.5	7.1	–	–	–	2.8	–	MSX
V762 Sgr	15.0	35.9	44.5	13.5	–	–	14.4	9.3	5.1	MSX
V407 Sco	9.8	18.1	19.4	6.1	–	–	5.6	3.8	–	MSX
ER Aql	34.4	61.5	62.3	10.1	–	–	6.9	4.7	–	MSX
V441 Cas	5.9	11.6	14.3	2.0	–	–	1.5	–	–	MSX
EO Cas	11.8	21.4	30.9	9.3	–	–	7.5	4.8	3.0	MSX
IW Cas	23.3	47.4	50.9	52.9	58.5	61.8	60.5	–	–	IRAS−LRS
CSS2 10	1.3	2.8	3.1	0.36	–	–	–	–	–	MSX
AU Car	5.9	9.0	10.3	2.1	–	–	–	–	–	MSX
RX Car	5.0	7.7	8.9	2.1	–	–	1.7	–	–	MSX
W And	368	643	591	185	198	163	143	–	–	IRAS−LRS
RR Mon	24.1	42.5	52.8	21.3	–	–	18.0	12.7	7.2	MSX
SU Pup	28.5	43.8	45.5	22.3	26.6	29.1	29.3	–	–	IRAS−LRS
UU Vel	23.5	46.9	51.6	13.6	–	–	11.5	7.5	4.1	MSX
RT Sco	285	460	512	162	–	–	163	108	67.4	MSX
V865 Aql	126	191	199	36.5	33.8	35.2	35.8	–	–	IRAS−LRS
RW And	95.9	132	131	48.8	52.8	53.0	50.1	–	–	IRAS−LRS
AK Mon	9.3	13.1	14.7	3.1	–	–	2.8	2.2	–	MSX
V745 Sgr	38.2	75.8	82.5	18.5	–	–	16.1	11.3	7.4	MSX
S Cyg	11.8	14.0	16.5	2.0	–	–	1.5	0.74	–	MSX
FF Cyg	37.8	65.8	82.0	8.5	–	–	6.4	4.9	–	MSX
FG Per	3.2	6.0	6.8	1.1	–	–	–	–	–	MSX
TT Cen	19.5	48.9	54.7	15.5	–	–	16.3	10.1	8.0	MSX
ST Sgr	97.7	148	149	61.6	63.2	61.1	56.4	–	–	IRAS−LRS
LX Cyg	14.2	28.0	44.9	10.2	–	–	9.4	5.1	–	MSX
VX Aql	13.5	33.6	37.7	9.3	–	–	10.6	6.8	3.5	MSX
V418 Cas	11.0	16.0	22.8	12.5	–	–	12.2	7.9	5.5	MSX

Table 9. Sample *C* − third part.

Source name	Var. type (GCVS)	Period (GCVS)	Distance (kpc)	Ref. distance	Bol. magnitudes $P-L$ method	I. − E.
T Cam	M	373.2	0.50	$P-L$ / this paper	−5.22	I
R Lyn	M	378.75	0.95	$P-L$ / this paper	−5.19	I
R Gem	M	369.91	0.66	$P-L$ / this paper	−5.23	I
WX CMi	M	420.1	2.35	$P-L$ / this paper	−5.31	–
S UMa	M	225.87	0.96	$P-L$ / this paper	−4.56	I
GI Lup	M	326.2	0.80	$P-L$ / this paper	–	I
WY Cas	M	476.56	0.97	$P-L$ / this paper	−5.50	I
X And	M	346.18	1.31	$P-L$ / this paper	−5.03	I
U Cas	M	277.19	1.08	$P-L$ / this paper	−4.74	I
GH Aur	M	349	2.64	$P-L$ / this paper	−5.13	I
TT CMa	M	314	1.08	$P-L$ / this paper	−4.95	I
EX Pup	M	289	3.02	$P-L$ / this paper	−4.92	–
RY Car	M	424.3	1.95	$P-L$ / this paper	−5.34	I
NZ Cen	M	382	2.22	$P-L$ / this paper	−5.17	I
R Cam	M	270.22	0.84	$P-L$ / this paper	−4.81	E
V762 Sgr	M	444	1.50	$P-L$ / this paper	−5.42	I
V407 Sco	M	396	2.11	$P-L$ / this paper	−5.26	I
ER Aql	M	337.6	1.04	$P-L$ / this paper	−5.10	I
V441 Cas	M	175.6	1.40	$P-L$ / this paper	−4.17	*E*
EO Cas	M	455	1.83	$P-L$ / this paper	−5.47	I
IW Cas	M	396.38	1.34	$P-L$ / this paper	−5.19	–
CSS2 10	M	250	3.78	$P-L$ / this paper	−4.69	–
AU Car	M	332	2.54	$P-L$ / this paper	−5.05	–
RX Car	M	332.8	2.75	$P-L$ / this paper	−5.04	–
W And	M	395.93	0.38	$P-L$ / this paper	−5.27	I
RR Mon	M	394.7	1.28	$P-L$ / this paper	−5.24	I
SU Pup	M	339.8	1.26	$P-L$ / this paper	−5.01	I
UU Vel	M	408.9	1.31	$P-L$ / this paper	−5.32	I
RT Sco	M	449.04	0.45	$P-L$ / this paper	−5.44	I
V865 Aql	M	364.8	0.62	$P-L$ / this paper	−5.18	–
RW And	M	430.3	0.86	$P-L$ / this paper	−5.36	–
AK Mon	M	328.6	2.12	$P-L$ / this paper	−5.02	–
V745 Sgr	M	380.2	0.99	$P-L$ / this paper	−5.23	–
S Cyg	M	322.93	1.94	$P-L$ / this paper	−5.06	I
FF Cyg	M	323.82	0.87	$P-L$ / this paper	−5.07	I
FG Per	M	340.3	3.16	$P-L$ / this paper	−5.10	–
TT Cen	M	462	1.39	$P-L$ / this paper	−5.48	–
ST Sgr	M	395.12	0.76	$P-L$ / this paper	−5.24	I
LX Cyg	M	465.3	1.53	$P-L$ / this paper	−5.51	I
VX Aql	M	604	1.99	$P-L$ / this paper	−5.87	I
		Zijlstra et al. (2004)				
V418 Cas	M	480	2.24	$P-L$ / this paper	−5.50	–

Table 10. Sample $D-$ distance estimates.

Source name	Apparent bol. magnitudes	Distance (kpc)	Min. – Max. distance (kpc)
NX Per	7.61	3.57	2.97–4.30
NU Pup	8.58	5.56	4.63–6.69
DK CMa	6.06	1.75	1.45–2.10
EW Pup	7.04	2.74	2.28–3.29
WY Pyx	5.01	1.08	0.90–1.29
V2434 Oph	4.95	1.05	0.87–1.26
V342 Ser	6.55	2.18	1.82–2.63
V471 Sct	5.85	1.59	1.32–1.91
V427 Sct	6.88	2.54	2.11–3.06
V1959 Cyg	6.47	2.11	1.76–2.54
PR Nor	4.51	0.85	0.71–1.03
PZ Vul	8.43	5.20	4.33–6.25
GY Lac	7.31	3.11	2.58–3.74
V928 Cas	8.22	4.73	3.93–5.69
V508 Aur	8.28	4.86	4.04–5.84
V1992 Cyg	7.90	4.07	3.38–4.89
V1850 Cyg	8.56	5.53	4.60–6.65
V1242 Cyg	8.12	4.50	3.74–5.41